ASSESSING ASCE-41 ACCEPTANCE CRITERIA FOR LINEAR AND NONLINEAR PROCEDURES USING INSTRUMENTED BUILDING DATA

Laura L. Hernández-Bassal and Sashi K. Kunnath

Department of Civil and Environmental Engineering

Abstract

Current provisions in ASCE-41 for performance-based assessment are applied to an existing three-story steel moment frame building that was designed and constructed prior to the 1961 UBC code revisions. A computer model of a perimeter frame that comprises the primary lateral system of the building was developed and validated against available instrumented data from two earthquakes. Both linear and nonlinear procedures were used in the assessment. Findings from the study indicate that the linear static and dynamic procedures produced consistent demand-to-capacity ratios. The nonlinear static procedure resulted in the most severe demands at the lowest level with two beams failing the Collapse Prevention limit state whereas the nonlinear dynamic procedure produced the lowest demands on the building; however, the fact that some individual motions caused some beams to exceed Life Safety or Collapse Prevention limits indicates that ground motion selection can play a major role in the outcome of the assessment when using the nonlinear dynamic procedure.

Introduction

The development of ASCE-41 (ASCE 2017) and other ongoing efforts directed towards the enhancement of performance-based codes represent a significant advancement in the practice of earthquake engineering. However, calibration and validation of the modeling parameters and acceptance criteria to real building performance is clearly needed for practicing engineers to gain confidence in the proposed methodologies. The use of strong motion data obtained from instrumented buildings experiencing strong ground shaking is an essential part of this process.

ASCE-41 permits as many as four analytical procedures to estimate seismic demands: Linear Static Procedure (LSP), Linear Dynamic Procedure (LDP), Nonlinear Static Procedure (NSP), and Nonlinear Dynamic Procedure (NDP). This implies that the assessment of a regular low to mid-rise building using any of the methods should reach the same conclusion on the performance of the system. Recently, Harris and Speicher (2018) carried out a detailed ASCE 41-based assessment of six modern steel frames varying in height from four to sixteen stories designed to the provisions of ASCE-7 (ASCE 2016). Their study identified numerous inconsistencies in the different evaluation procedures: for example, LDP consistently resulted in lower demand-to-capacity ratios (DCRs) than LSP and likewise NSP consistently resulted in lower DCRs than NDP – though it is recognized that nonlinear responses are sensitive to model and analysis parameters.

The results reported in this paper are part of a larger study investigating three instrumented buildings and examining several ASCE-41 provisions. It can be viewed as an extension of the study by Harris and Speicher to an existing building where the numerical model has been calibrated to observed responses.

Building and Instrumentation Data

The first structure selected for assessment is a 3-story office building designed in 1958 and located in San Bernardino, California. The structure is composed of moment frames along the exterior serving as the lateral load resisting system in both directions. The gravity system is a wood truss-joist system supported on steel columns that spans in the north-south direction. Figure 1 shows the plan view of the building and the elevation of the perimeter frame used in the assessment.
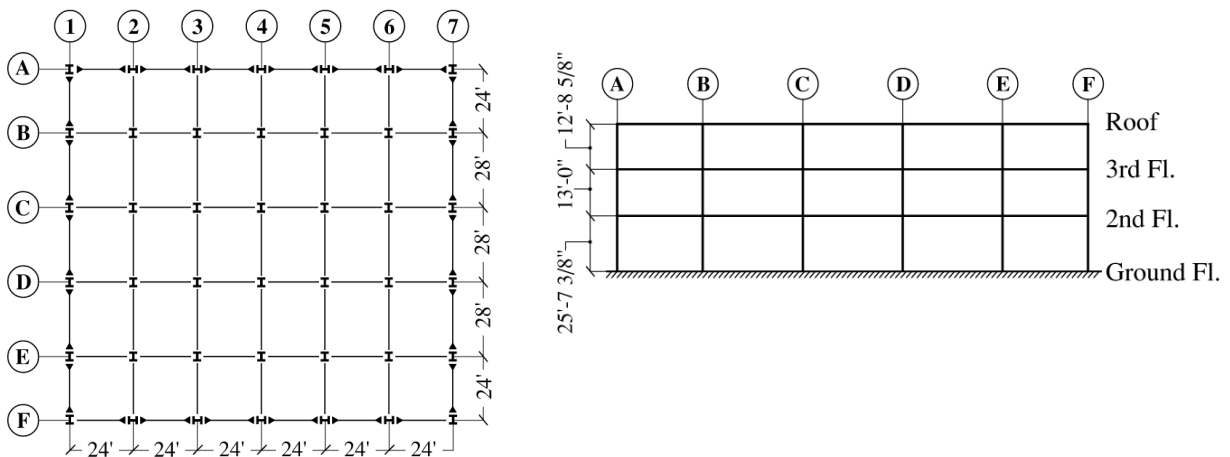

Figure 1. Plan view of building and elevation of perimeter frame on line 1

The building has been instrumented by the California Strong Motion Instrumentation Program (CSMIP Station 23516) with thirteen accelerometers: three at the ground level to record base accelerations in all three orthogonal directions, three each at the 2nd floor and roof, and four at the third level of the building – as shown in Figure 2.
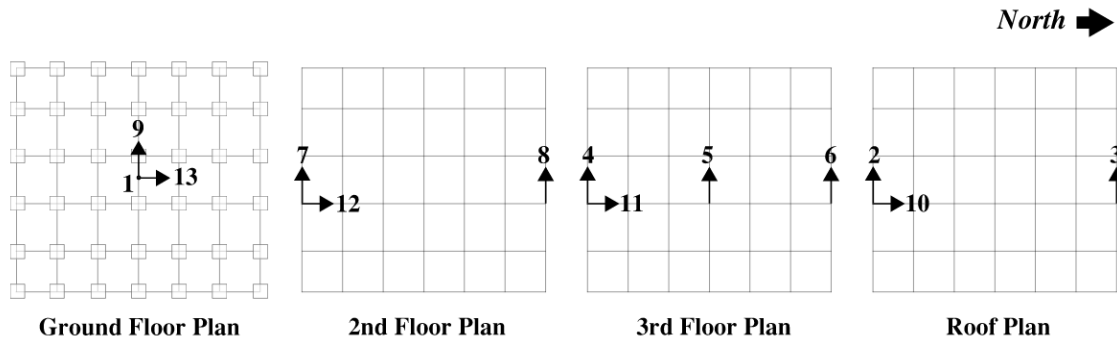

Figure 2. Locations of installed sensors

Instrumented data from several earthquakes are available for this building, as indicated in Table 1. Of the available data, two recorded motions with the highest ground peak accelerations

(PGA) were selected to calibrate the simulation model: Landers (1992) and San Bernardino (2009).

Table 1. Available instrumented data for selected building

Earthquake	Year	Peak Acceleration (g)	
		Ground	Structure
Landers	1992	0.110	0.280
San Bernardino	2009	0.102	0.155
Chino Hills	2008	0.052	0.076
Lake Elsinore	2007	0.036	0.050
Whittier	1987	0.030	0.090
Calexico	2010	0.022	0.108
Borrego Springs	2016	0.019	0.062
Borrego Springs	2010	0.018	0.077
Inglewood	2009	0.010	0.029
Beaumont	2010	0.009	0.016

When examining the time series for the Landers earthquake, unusual long-period content was observed throughout the record, particularly in the floor displacement histories (see roof history shown in Fig. 3). Therefore, a high-pass filter was applied with a corner frequency of 0.5 Hz using an 8th order zero phase delay Butterworth filter. Figure 3 shows the base acceleration as well as the relative roof displacement before and after filtering.
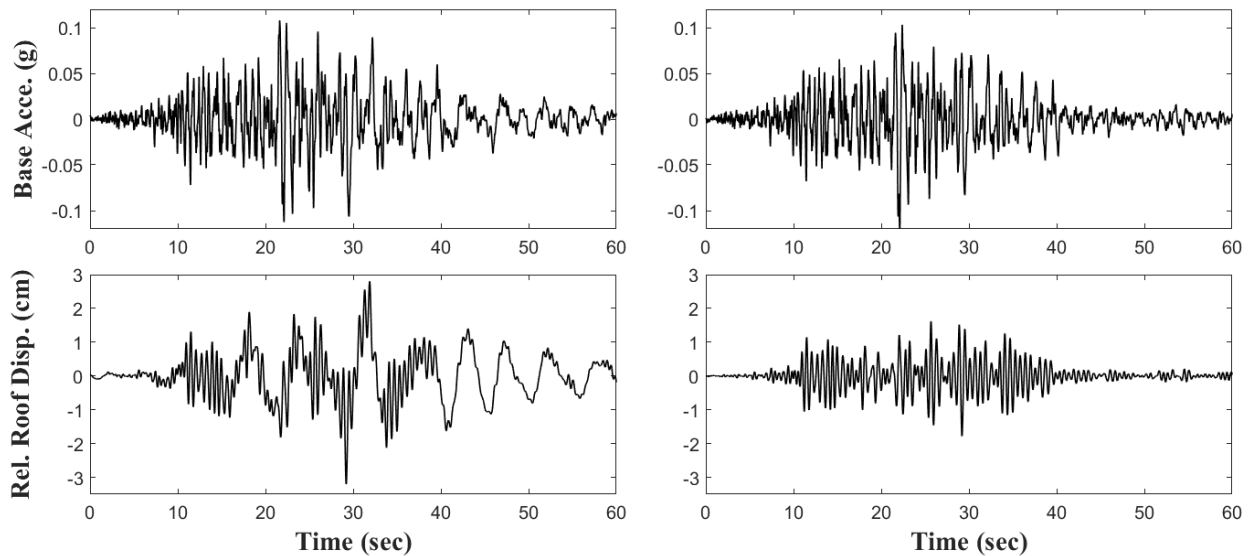

Figure 3. Unfiltered (left) and filtered (right) time histories

Modeling and Validation

Given the general symmetry of the building plan and the fact that torsional motions were not evident in the profile of the recorded floor displacement histories, the analyses were carried out on a two-dimensional model (Fig. 4) of the perimeter moment frame in the east-west direction.
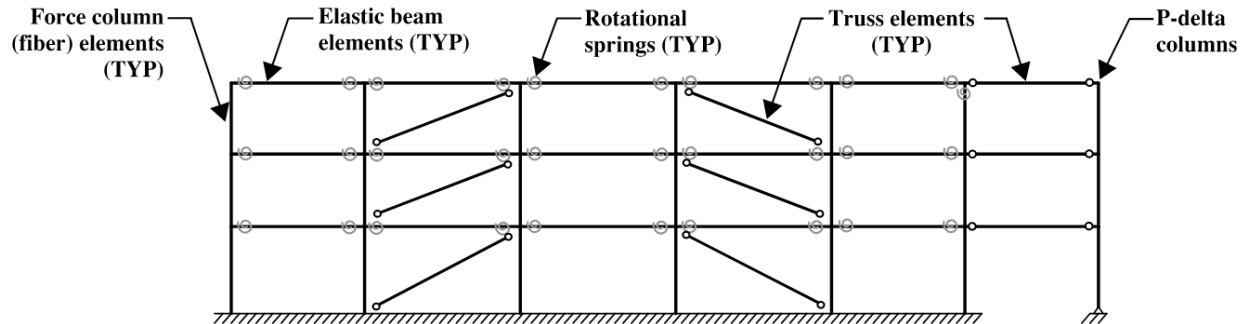

Figure 4. Two-dimensional model of perimeter frame used in assessment

Beams are modeled using elastic beam-column elements with inelastic springs (constructed with zero-length elements) at the ends as shown in Figure 4. All inelastic action (for nonlinear procedures) is lumped into these concentrated springs whose cyclic response is represented using the Modified Ibarra-Medina-Krawinkler deterioration model (Ibarra et al. 2005). In order to capture the axial load-moment interaction, columns were modeled as force-based elements with five Lobatto integration points and the Voce-Chaboche material model was used to represent the inelastic cyclic behavior of steel. Center-line dimensions are used for beams and columns to indirectly account for the flexibility of the panel zones. The building has embedded column bases connected to spread footings and grade beams and therefore the base was assumed to be fully restrained – an assumption that was shown to be reasonable for such a base connection (Falborski et al. 2020). An additional leaning column is attached to the moment frame using rigid links with pinned connections at each end to account for P-Delta effects and contributing gravity loads from the interior frames are applied at each level. A set of diagonal braces were also added at each level to represent the stiffness contribution of non-structural elements – the process by which the brace stiffness was determined is described in the following section.

Calibration of Non-Structural Stiffness

An eigenvalue analysis was carried out on the bare frame structure without the diagonal braces and the fundamental period of the structure was estimated as 0.70 sec. A Fast Fourier Transform (FFT) was carried out using the acceleration time histories at each level and Transfer Functions (relative to the base) were obtained for both the Landers and San Bernardino earthquakes. The resulting plots for the Landers recordings are shown in Fig. 5 where a predominant frequency is evident at approximately 1.8 Hz or a period of 0.56 sec.
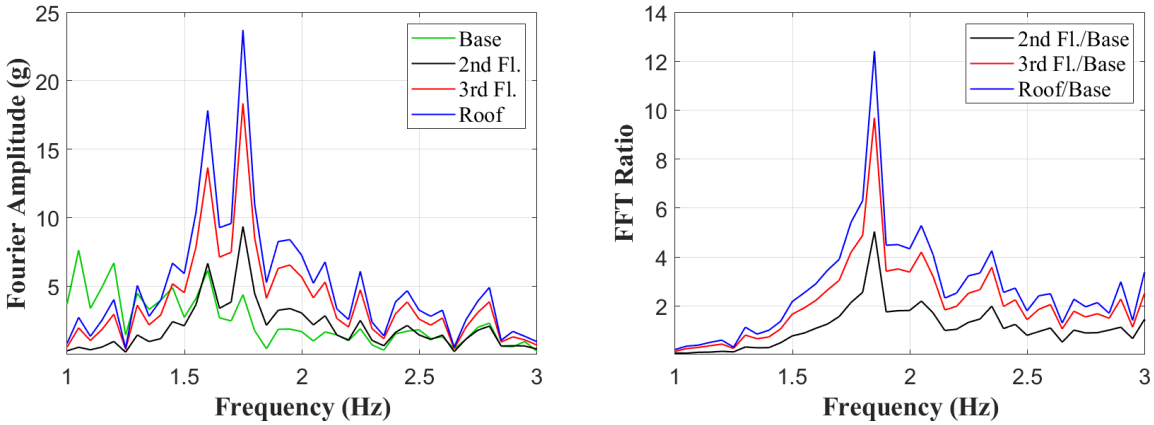
Figure 5. Fourier transform and transfer functions from acceleration histories recorded during Landers earthquake

The procedure outlined in Falborski et al. (2020) was utilized to establish the non-structural stiffness at each story level. At any time instant during the dynamic response of the structure, the shear in any story K can be estimated from:

$$V_k^{story}(t) = V_K^{NS}(t) + V_K^{STR}(t) + C_K \cdot \dot{\Delta}_K(t)$$
$$= \sum_{i=K}^{N} m_i \, \ddot{u}_i(t) \tag{1}$$

In the above equation, $V_K^{story}(t)$ is the instantaneous shear in story K at time t, $V_K^{NS}(t)$ and $V_K^{STR}(t)$ are the story shears from the non-structural and structural components, respectively, $C_K \cdot \dot{\Delta}_K(t)$ is the story force due to damping, and $\sum_{i=K}^{N} m_i \, \ddot{u}_i(t)$ is the sum of the inertia forces above story K.

Using the recorded time histories, the time instants at which the interstory velocities are zero are determined for each story K. At these instants, the damping force is eliminated in Equation (1). The lateral displacements at each floor corresponding to these time instants are determined and applied statically to the model. The resulting shears will be structural story shears at each level. The total shear is determined by summing the inertia forces above that level, hence the non-structural contribution can be established. At each time instant when the interstory velocity is zero, the nonstructural story shear can be plotted vs. the corresponding interstory drift at story K. Linear regression can be used to fit the data points and the resulting slope represents the nonstructural story stiffness. Likewise, the total and structural stiffness at each floor can be estimated using a similar approach. The estimated story stiffnesses are shown for a typical floor in Fig. 6 for the San Bernardino recordings. Table 2 lists the numerical values of the estimated stiffness quantities.
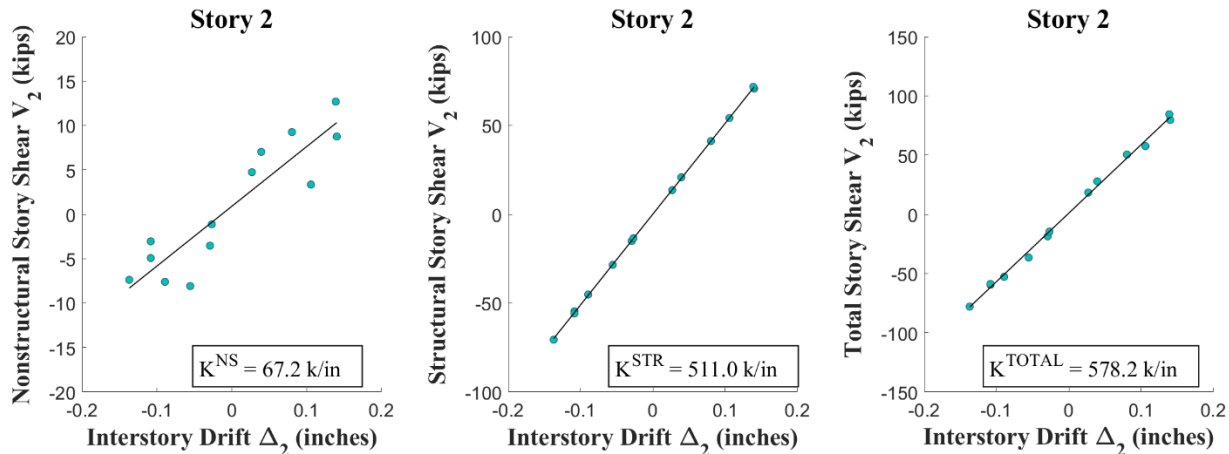
Figure 6. Estimating non-structural stiffness for a typical story
(Data from San Bernardino earthquake)

In order to add the nonstructural stiffness, braces were introduced in two bays at each floor through the use of truss elements as shown previously in Fig. 4. The properties of the braces were adjusted until the total story stiffness matched the calculated values shown in Table 2. This was accomplished iteratively by updating the areas of the braces, applying static lateral loading to the model and determining the total story stiffness. The addition of the braces to the model as well as incorporating the additional stiffness of the joist floor system altered the fundamental period of the frame to 0.54 sec, consistent with the estimated building period in the east-west direction from the FFT analysis (Fig. 5).

Table 2. Estimated components of story stiffness

Story	Stiffness (k/in)			
	K^{NS}	K^{STR}	K^{TOTAL}	K^{NS}/K^{TOTAL}
1	51.9	551.1	603.0	0.09
2	67.2	511.0	578.2	0.12
3	102.9	340.3	443.2	0.23

Calibration of Damping

The concept behind Equation (1) can also be used to calibrate damping. In this case, the time instants at which the interstory drifts are zero are considered. Therefore, the total damping force in any story at these time instants will be equal to the sum of the inertia forces above that story. However, the damping coefficients will correspond to the lateral degree-of-freedom of the floor and additional calibration will be needed to establish Rayleigh coefficients associated with the mass and stiffness matrices of the system. Hence, in the present study, damping was estimated using the logarithmic decrement method by examining the displacement histories of the floors at the end of the recordings. Shown in Figure 7 are the floor displacement histories at the end of the recording during the San Bernardino earthquake which is assumed to represent the free vibration phase of the response. The decay in the response over the final two cycles is used to estimate damping. The estimated damping ratio varies from 13% in the first floor to 19% in the third floor. The high damping obtained with this approach indicated some anomaly in the

data and/or assumption about the free vibration phase. Hence, an additional method was utilized to estimate damping – the analysis model (with nonstructural stiffness already calibrated) was subjected to both the Landers and San Bernardino base motions and the response spectra, based on the roof accelerations, was compared to that obtained with the actual recorded motions. Results are presented in Fig. 8 which suggest that a damping of 10% (assigned to both the 1st and 2nd mode) produced a reasonable match. Hence the time history simulations presented in this paper are based on Rayleigh damping with coefficients corresponding to 10% of critical damping in the 1st and 2nd mode.
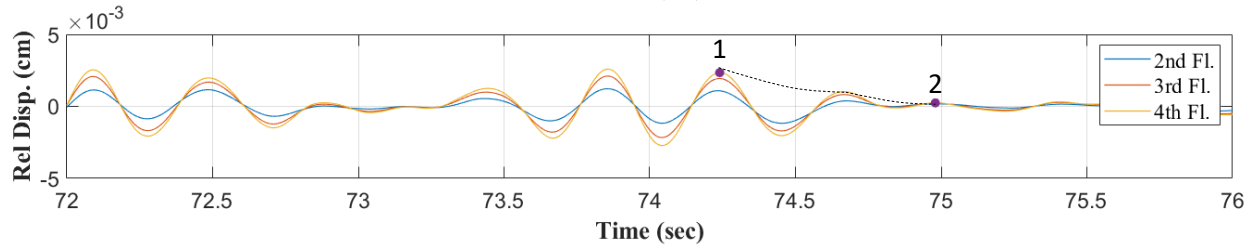

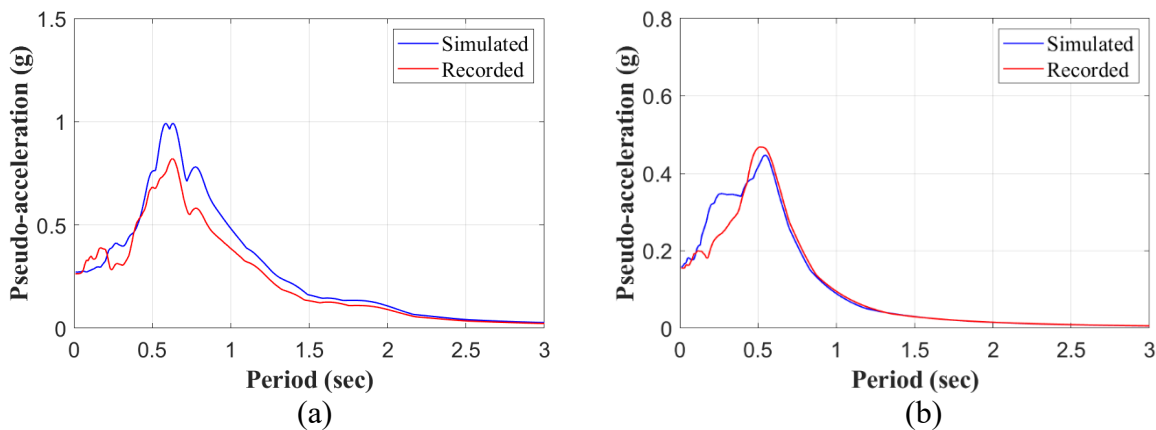**Figure 7. Free vibration response following the San Bernardino earthquake**

(a)   (b)

Figure 8. Comparison of acceleration spectra using data from the roof response:
(a) Landers; (b) San Bernardino

Model Validation

The model was calibrated assuming elastic behavior during each of the recorded motions based on the following facts: (1) the fundamental period did not shift during these motions, and (2) there was no evident structural damage in the building following the seismic events. The simulated and recorded roof displacement histories during the Landers and San Bernardino shaking are shown in Fig. 9. The peak displacements during the Landers earthquake is slightly over-estimated – this is attributed to the fact that the 10% damping used in the simulation was lower than the observed damping (see Fig. 8). The magnitude of the response during the San Bernardino earthquake was negligible during the first 25 seconds, hence roof displacement history is shown beyond this point.
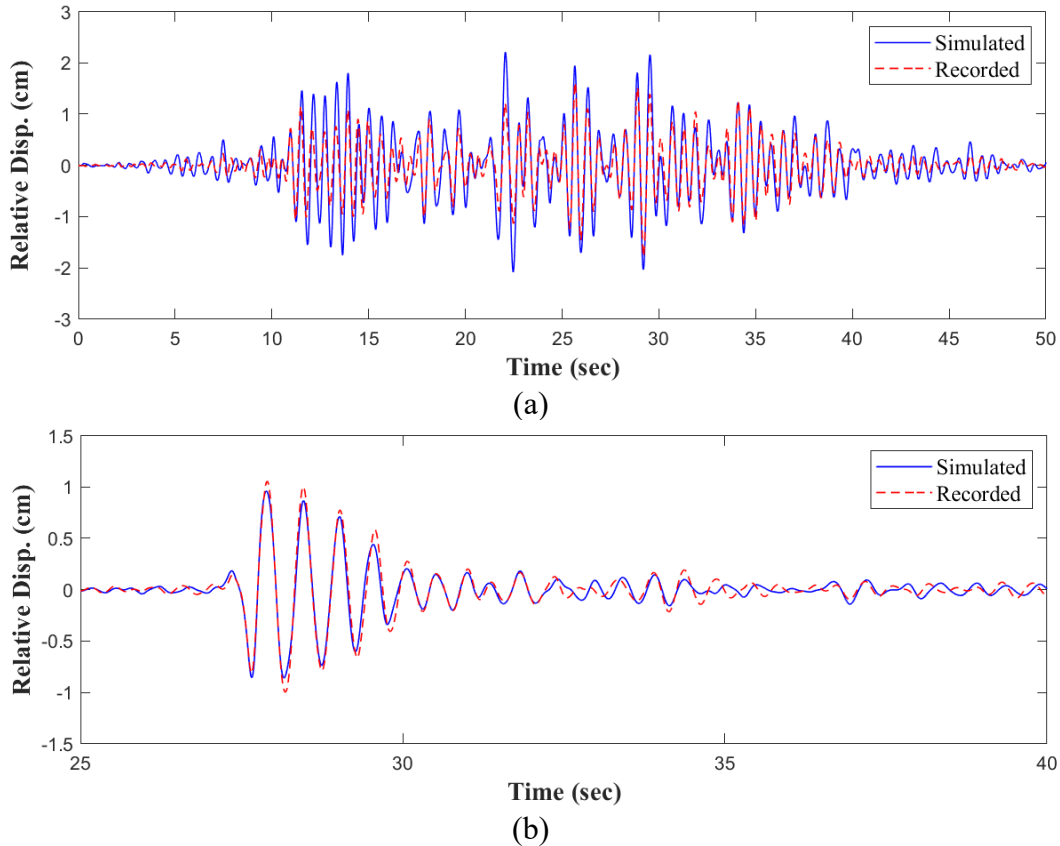
Figure 9. Comparison of recorded vs. simulated roof displacement histories:
(a) Landers; (b) San Bernardino

Building Assessment using ASCE 41 Guidelines

A seismic performance assessment of the building was carried out by analyzing the validated computer model of the perimeter frame and using both linear and nonlinear analysis procedures prescribed in ASCE 41. Note that in all procedures described hereafter, the lateral load application is preceded by the application of the sustained gravity loads on the frame. The seismicity considered in the assessment is based on the BSE-2E hazard level, which represents a 50% probability of occurrence in 50 years. The resulting response spectrum for the site is shown in Fig. 10 with the following key parameters: S_{XS} = 1.9 g; S_{X1} = 1.25 g; T_O = 0.13 sec and T_S = 0.66 sec.
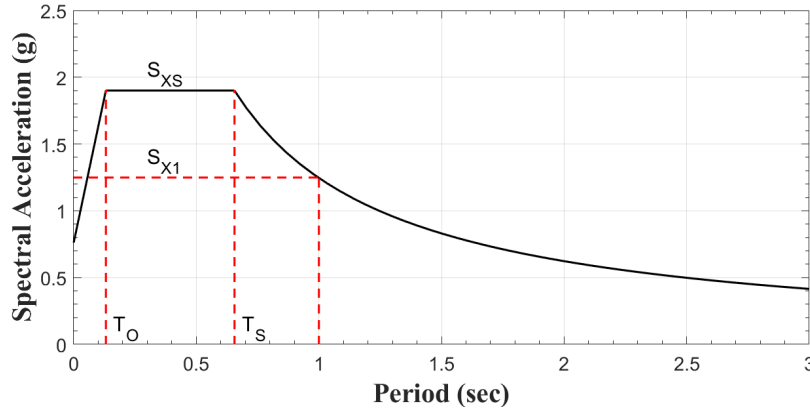
Figure 10. Response spectrum for site

Linear Procedures

For the Linear Static Procedure (LSP), an equivalent static load, representative of the seismic hazard, is applied over the height of the building. First, the pseudo lateral force V is calculated by using the following expression provided in ASCE 41:

$$V = C_1 C_2 C_m S_a W \qquad (2)$$

The modification factors that account for inelastic behavior C_1 and hysterisis characteristics C_2 were both determined to be 1.0, whereas the effective mass factor $C_m = 0.9$. The spectral acceleration S_a was obtained from Fig. 10. The effective seismic weight of the building is 2058 kips and half this value was used to estimate the total lateral load on the perimeter frame. All elements were deformation-controlled, hence the maximum moment demands in each element was obtained due to the applied lateral forces and the corresponding demand-to-capacity ratios (DCRs or m-factors) are plotted in Fig. 11 (a) and 12 (a).

For the Linear Dynamic Procedure (LDP), the assessment was based on the response spectrum method. Considering the first three modes was sufficient to capture at least 90% of the participating mass of the frame. The equivalent static lateral load vector was then determined from:

$$\{p\} = [m]\{\Phi\} \Gamma S_a \qquad (3)$$

where $[m]$ is the lumped mass matrix, $[\Phi]$ is the modal vector, Γ is the modal participation factor, and S_a is the spectral acceleration at the fundamental period of the frame, obtained from the target response spectrum (Fig. 10). Peak responses are recorded for each set of lateral loads and the modal demands are combined using the square root sum of squares (SRSS). The DCRs are shown in Fig. 11 (b) and 12 (b) alongside the LSP results. It is seen that both linear procedures produce very similar DCR values – several beams exceed Life Safety (LS) performance level at the lower two levels whereas the columns exhibited much better performance just exceeding Immediate Occupany (IO) limits at the first floor level.
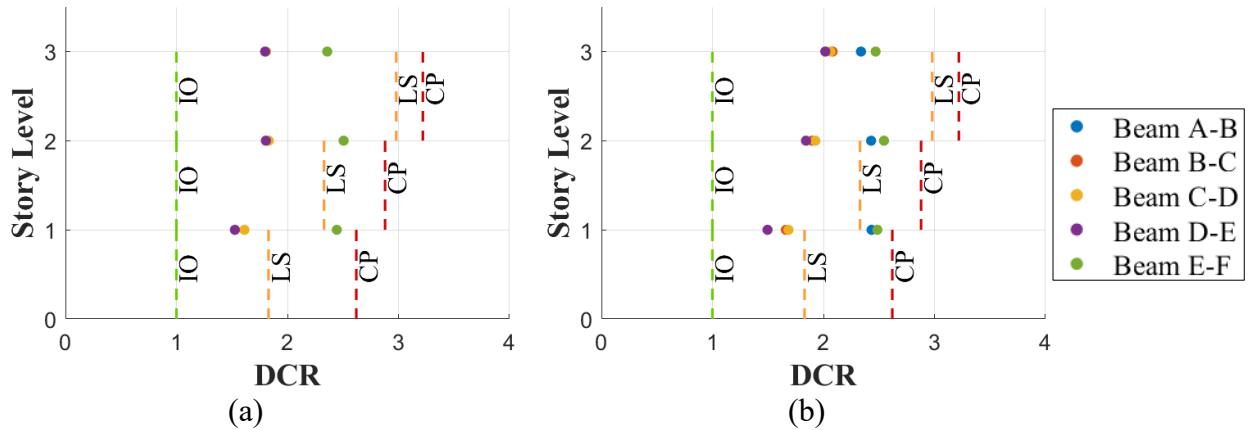
(a)   (b)

Figure 11. Demand-to-capacity ratios for beams:
(a) Linear Static Procedure; (b) Linear Dynamic Procedure
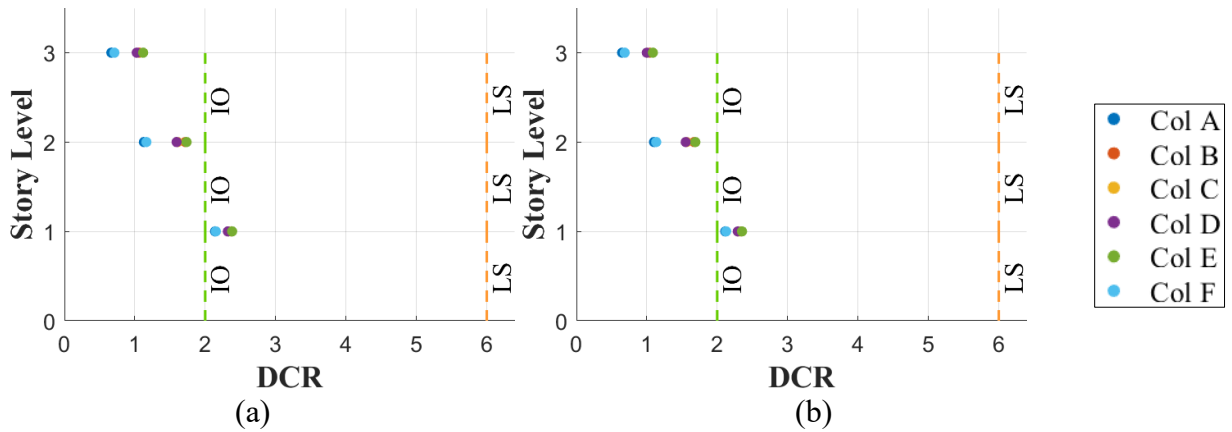

(a)   (b)

Figure 12. Demand-to-capacity ratios for columns:
(a) Linear Static Procedure; (b) Linear Dynamic Procedure

Nonlinear Procedures

As described previously, nonlinear action in the beams is represented by concentrated springs while columns are modeled using distriuted plasticity elements with fiber sections to capture axial force-moment interaction effects. The response of each nonlinear spring is based on the Modified Ibarra-Medina-Krawinkler (I-K) model – the transformation of the I-K model into the ASCE 41 backbone envelope for use in nonlinear procedures is displayed in Fig. 13.
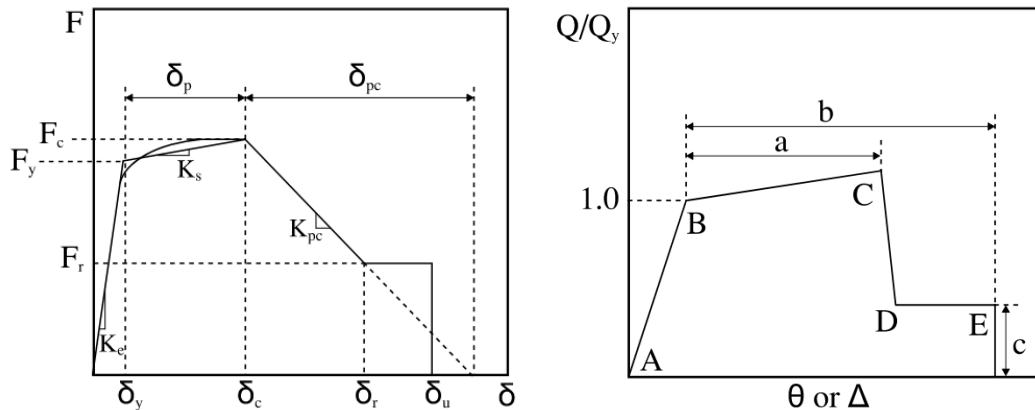
Figure 13. Modified Ibarra-Medina-Krawinkler model (left) and transformed backbone parameters (right) used in nonlinear procedures

For the Nonlinear Static Procedure (NSP), the target displacement δ_t is calculated using:

$$\delta_t = C_0 C_1 C_2 S_a \frac{T_e^2}{4\pi^2} g \tag{4}$$

The modification factors that accounts for the multi to single degree-of-freedom transformation, inelastic behavior, and hysteretic characteristics, respectively, were determined to be: $C_0 = 1.3$, $C_1 = 1.034$ and $C_2 = 1.0$. The effective fundamental period, and consequently the target displacement, was estimated through an iterative process to establish a converged effective period. The final computed target displacement was 11.28" (corresponding to a roof drift of 2.3 %) and an effective to initial stiffness ratio of 1.24. The inelastic demands in the beams and columns at the target displacement are estimated using OpenSees and are compared to the ASCE 41 acceptance criteria in Fig. 15 (a) and Fig. 16 (a).

Ground Motion Selection for NDP

In order to select ground motions that are representative of the seismic hazard at the site, the United States Geological Survey (2017) *Unified Hazard Tool* was used for the site deaggreation. The hazard at the site is controlled primarily by the San Jacinto fault with expected magnitude 8.0 and fault distances less than 1 km and the San Andreas fault with magnitude range 7.0 – 8.0 and fault distances between 7 – 12 km. A total of 51 ground motions were downloaded from the PEER NGA ground motion database (ngawest2.berkeley.edu) with the following filters: fault type: strike slip; magnitude: 6 to 8; distance to rupture: 0 to 12; and shear wave velocity Vs30: 180 to 360 m/s. Ground motions with spectral shapes signficantly different from the target spectrum were discarded. The final 11 sets of ground motion (pairs) were selected such that the average maximum direction spectra (RotD100) was at or above 90% of the target response spectrum in the period range $0.2T_1 – 1.5T_1$. Given that the site is classified as near-fault, the horizontal components of each selected set was rotated to the fault-normal and fault-parallel directions of the causative fault. The fault closest to the site is the San Jacinto fault, hence this fault angle was used as the reference for rotating the ground motions. ASCE 41-17 does not provide specific guidance on ground motion selection for 2D analysis. Therefore, the following procedure was implemented: for each ground motion set already rotated in the fault parallel and normal orientations, the base motions and their spectra in each direction were compared; the

motion with a larger evident pulse in the time history or a larger spectral value within the target period range was selected. A additional scale factor of 1.1 was necessary to ensure that the actually applied ground motions had a mean spectra that was equal to or above the target spetrum in the required period range. Figure 14 shows the final ground motion spectra and Table 3 summarizes essential details of the selected records.
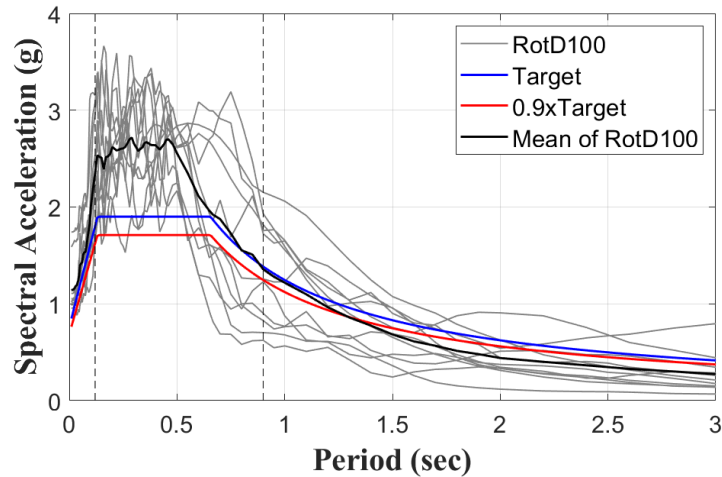

Figure 14. Maximum direction spectra of scaled motions and comparison of mean spectrum with target spectrum at site

Table 3. Selected ground motions

GM #	Record Sequence Number	Earthquake Name	Year	Station Name	Magnitude	R_{rup} (km)
1	6	"Imperial Valley-02"	1940	El Centro Array #9	6.95	6.1
2	30	"Parkfield"	1966	Cholame-Shandon Array #5	6.19	9.6
3	95	"Managua_-Nicaragua-01"	1972	"Managua_ ESSO"	6.24	4.1
4	162	"Imperial Valley-06"	1979	"Calexico Fire Station"	6.53	10.5
5	165	"Imperial Valley-06"	1979	"Chihuahua"	6.53	7.3
6	185	"Imperial Valley-06"	1979	"Holtville Post Office"	6.53	7.5
7	558	"Chalfant Valley-02"	1986	"Zack Brothers Ranch"	6.19	7.6
8	725	"Superstition Hills-02"	1987	"Poe Road (temp)"	6.54	11.2
9	4098	"Parkfield-02_ CA"	2004	"Parkfield - Cholame 1E"	6.00	3.0
10	4102	"Parkfield-02_ CA"	2004	"Parkfield - Cholame 3W"	6.00	3.6
11	4108	"Parkfield-02_ CA"	2004	"Parkfield - Fault Zone 3"	6.00	2.7

Nonlinear simulations of the calibrated numerical model were carried out using OpenSees for each of the eleven ground motions, and mean values of the plastic rotations in the beams and columns at each end of the element were determined. The maximum plastic rotation among all eleven motions was also recorded. Results are presented in Fig. 15 (b) and Fig. 16 (b) alongside the estimates from NSP. Two beams at the first floor level fail the Collapse Prevention (CP) limit when using NSP but pass Immediate Occupancy (IO) under NDP when considering the average rotation for the eleven motions. If the peak rotation among all motions are considered, the LS limit was exceeded in two beams and the CP limit was exceeded in one beam at the first floor level. Column demands in general were small and meet or slightly exceeded the criteria for IO performance level at all levels for both NSP and NDP.
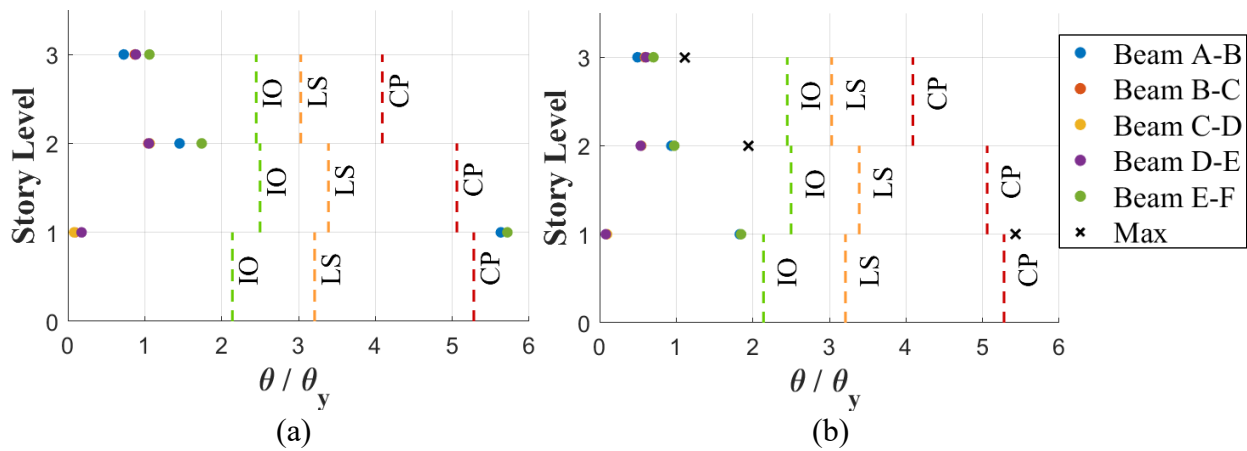

Figure 15. Ductility demands for beams:
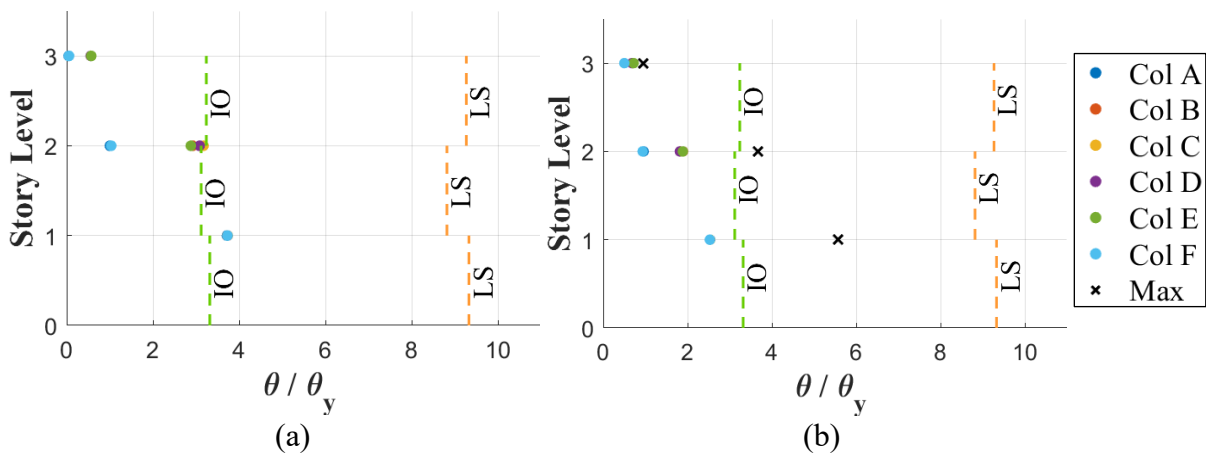**(a) Nonlinear Static Procedure; (b) Nonlinear Dynamic Procedure**

Figure 16. Ductility demands for columns:
(a) Nonlinear Static Procedure; (b) Nonlinear Dynamic Procedure

Conclusions

An existing three-story steel moment frame building that was designed and constructed prior to the 1961 UBC code revisions was analyzed using the modeling and acceptance criteria

outlined in ASCE-41. Significant effort was directed towards identifying the nonstructural stiffness of the system, estimating damping and validating the computer model of the perimeter frame used in the assessment of the building.

Results of the simulations indicate that both linear procedures resulted in consistent DCRs for both beams and columns at all floor levels. The nonlinear static procedure resulted in the most severe demands at the first floor with two beams failing the CP limit state. Simulations using NDP resulted in the lowest demands when considering the mean demands for all eleven ground motions. However, when the response to individual motions are examined, beams on the first floor failed LS performance in two cases and CP performance level in one event. This highlights the importance of ground motion selection and scaling when using NDP.

Acknowledgements

References

ASCE (2017). Seismic Evaluation and Retrofit of Existing Buildings, ASCE/SEI 41-17, American Society of Civil Engineers, Reston, Virginia.

ASCE (2016). Minimum Design Loads and Associated Criteria for Buildings and Other Structures, ASCE/SEI 7-16, American Society of Civil Engineers, Reston, Virginia.

Falborski, T., Hassan, A.S., Kanvinde, A.M (2020). Column Base Fixity in Steel Moment Frames: Observations From Instrumented Buildings, Journal of Constructional Steel Research. 168. 105993. 10.1016/j.jcsr.2020.105993.

Harris, J. and Speicher, M. (2019). Assessment of Performance-Based Seismic Design Methods in ASCE 41 for New Steel Buildings: Special Moment Frames, Earthquake Spectra. **34** (3).

Ibarra, L. F., and Krawinkler, H. (2005). Global Collapse of Frame Structures under Seismic Excitations. Technical Report 152, The John A. Blume Earthquake Engineering Research Center, Department of Civil Engineering, Stanford University, Stanford, CA.

U.S. Geological Survey (2017). Unified Hazard Tool, accessed September 7, 2020 at URL https://earthquake.usgs.gov/hazards/interactive/